JOURNAL OF GUIDANCE, CONTROL, AND DYNAMICS
Vol. 32, No. 2, March–April 2009

Fast Model Predictive Control of the Nadir Singularity in Electro-Optic Systems

David Anderson* and Meghan McGookin†
University of Glasgow, Glasgow, Scotland G12 8QQ, United Kingdom
and
Nick Brignall‡
SELEX Sensors and Airborne Systems, Edinburgh, Scotland EH5 2XS, United Kingdom

DOI: 10.2514/1.30762

Civilian airborne directed-countermeasure electro-optic systems require the simplest, most affordable, sightline pointing and stabilization system: a two-axis gimbal. Two-axis gimbal tracking and jamming effectiveness degrades as the line of sight approaches the outer gimbal axis: the gimbal lock, keyhole, or nadir singularity condition. Our novel implementation of fast model predictive control in the position loop minimizes the tracking error by predicting the singularity. A second novel algorithm predicts the future set-point trajectory. This predictive controller yields near-optimal tracking performance without a priori slew-rate knowledge.

I. Introduction

PRECISION pointing and stabilization of the sightline are vital capabilities in all airborne electro-optic (EO) equipment. In traditional control theory terminology, the pointing task is a *tracking* requirement, either of a dynamic target or some other special point of interest, and stabilization refers to the *disturbance rejection* capability of the sightline controller; typical disturbances are a combination of ownship motion and bearing friction. The relative importance between the pointing and stabilization tasks is a function of the intended operation of the EO system; for example, long-range targeting requires precise stabilization, but an agile sightline is essential for directed infrared countermeasures (DIRCM) systems [1], although both pointing and stabilization loops should be optimized for all systems. A DIRCM engagement occurs when the host platform is attacked by a surface-to-air missile, usually a shoulder-launched Man-Portable Air Defence missile, which is defeated when the DIRCM system positions a jamming signal onto the missile seeker. Obviously, accurate target tracking is essential over a full hyper-hemispherical field of regard (FOR), as any tracking deficiencies are sure to be exploited by future missile guidance systems and tactics. Given the particular threat of global terrorism to the airline industry, future DIRCM systems should be small, lightweight, and cost-effective for inclusion on commercial aircraft, which invariably limits the number of available axes for sightline control.

A minimum of two axes are necessary to attain full hyper-hemispherical FOR. The outer gimbal (OG) axis is usually constrained to rotate with respect to the platform z axis (through azimuth angle η) and the inner gimbal (IG) with respect to the OG y axis (through elevation angle ε). This is shown in Fig. 1. When the outer and inner axes are orthogonal, the sightline can be positioned to any orientation in space, as the IG and OG axes form an ideal orthogonal basis. However, when the inner gimbal angle approaches the nadir (defined as $\varepsilon = -90\,\mathrm{deg}$) (i.e., the sightline becomes aligned with the axis of rotation of the outer gimbal), the pointing system experiences the loss of a degree of freedom known as *gimbal lock* and, as a result, the sightline cannot be arbitrarily positioned [2]. To guarantee tracking close to the nadir, the outer gimbal has to follow a large (theoretically infinite) acceleration demand, beyond the capability of any practical servomechanism. As a result, this leads to a significant tracking error and if this error exceeds the instantaneous field of view of the sensor, the track will be lost. This region inside which accurate tracking is impossible is known as the *nadir cone*. More important, if the missile sensor is not accurately tracked, the efficacy of the DIRCM defeat laser will be significantly impaired. This situation obviously has severe operational implications for the survivability of the host platform.

A number of solutions to the nadir problem exist using various approaches to either avoiding or mitigating the effect of the singularity [3–6]. Conceptually, the simplest tactic is to orient the axes of the turret such that the nadir singularity lies outside the operational region of the system [5]. However, this approach is unsuitable for a DIRCM system due to the need for hyperhemispherical coverage. The second method, also an optomechanical solution, is to add additional axes to the pointing and stabilization system. Unfortunately, this approach increases the size, complexity, and initial unit price, in addition to comparatively reducing the mean time between failure and hence raising operational costs. The third approach is to reduce the size of the nadir cone by using faster, more powerful, components in the gimbal actuation mechanism, with the inevitable financial penalties.

The fourth approach and the one investigated in this paper is the use of nonconventional sightline controllers to mitigate the effect of nadir singularity on tracking error. A number of techniques have been proposed, particularly for the design of satellite tracking antennas for which the singularity is known as the zenith *keyhole* [3–5]. Although many disparate nadir controllers exist (bespoken designs for specific systems) most can be broadly categorized as either a path replanning method or a shooting method. In a path replanning method, the desired sightline trajectory is altered to avoid the nadir singularity at the expense of tracking error [6,7]. In the shooting method, an open-loop control strategy is used to fire the sightline through the nadir by taking preemptive control action. Comparison studies, such as Crawford and Brush [4], have shown that the shooting method is the more accurate approach.

Although a significant body of work exists in this area, most of the antenna and satellite controllers proposed in the literature thus far have been tailored to specific nadir geometry, rather than being developed from within an online optimal control framework. This is because in the space systems tracking problem, the orbital slew rate and orbit plane (which define the nadir cone geometry) are known a priori and have very small temporal variations: information that is

Received 1 March 2007; revision received 3 July 2008; accepted for publication 4 July 2008.

*Lecturer, Department of Aerospace Engineering; d.anderson@aero.gla.ac.uk.
†Research Assistant.
‡Chief Engineer.

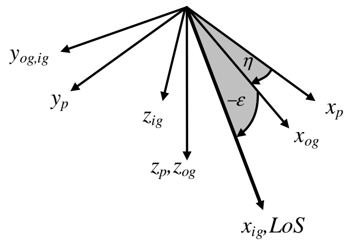

Fig. 1 Elevation over azimuth gimbal axes; subscript *p* denotes platform axes (LoS denotes line of sight).

not available a priori in the DIRCM scenario. Here, the nadir geometry must be computed optimally online.

One optimal controller synthesis technique possibly well suited to the nadir problem is model predictive control (MPC) [8]. MPC uses an internal model of the plant to predict the response over a finite receding horizon in time and with this information an optimal linear quadratic control strategy can be found to minimize tracking error over the prediction horizon. By formulating the optimization as a quadratic program (QP), constraints can be directly included in the optimization [8,9]. Therefore, MPC both implicitly embeds preemptive control action and optimally handles system constraints, the two essential properties of a nadir controller. However, there is a practical limit imposed by the QP solvers (such as numerical errors that may occur in very large matrices and excessive computational load). In the paper by Bemporad et al. [10], they have demonstrated that the real-time linear MPC problem can be formulated as a multiparametric quadratic program and solved explicitly with controllers designed for every location in the state space. Upon commissioning, the predictive controller is then implemented as a lookup table. This process is complicated for all but the simplest systems [11] (low plant order and small prediction horizon) and research is at the early stages. Fortunately for the nadir problem, an alternative control architecture, proposed here, can be used to test the efficacy of MPC.

Most high-performance servomechanism controllers are constructed from three nested loops: an inner current loop to provide accurate torque, a rate loop for stabilization, and a position loop for angle tracking. The purpose of the angle loop is to provide a demand signal to the rate loop, a signal that is implicitly constructed within the MPC solution. It is therefore a valid approach to replace the track loop compensator with an MPC controller and to use the internal model rate state to drive the actual gimbal rate loop. As the control signal is not to be used directly, a simpler model (run at a low sample rate) can be used to reduce the computational burden. To prevent any undesirable oscillations in the rate signal, a multirate stage may be employed to convert from the model to gimbal sample rates. The MPC controller now replaces the actual kinematic trajectory imposed by the engagement with one that optimally minimizes the tracking error subject to the receding horizon and the servo constraints.

The contributions of this paper are then threefold: First, a new approach to implementing MPC for fast systems with nested dynamics is presented. Second, a new algorithm for predicting the kinematic trajectory over the nadir is given. Third, the operational benefits of implementing a receding-horizon controller for a DIRCM system operating within the nadir region are examined.

II. System Models

A. Nadir Trajectory Generator (η_{dem})

Any predictive strategy requires estimates of the demands for a period of time into the future (the prediction horizon). For a tracking task, this is not generally possible, but the DIRCM scenario is such that because the crossing rate of the target as seen from the aircraft is low, the high gimbal rates that create the control problem are due to aircraft maneuvers. For the purposes of visualization, it is convenient to consider roll rotation of the aircraft when the gimbals are mounted such that the azimuth axis is substantially perpendicular to the roll axis; however, the analysis presented subsequently is general and uses *only* measurements of the two gimbal angles over a short time period to predict future angles.

During aircraft rotation, the position of the target relative to the aircraft is described by a circle (Fig. 2). The future position is predicted by extrapolating the circular motion into future time, with the assumption that the aircraft rotation rate is constant over the prediction horizon. The assumption of constant or known disturbances throughout the prediction horizon is required by both the trajectory generation algorithm described here and predictive control techniques in general. However, this is not a significant limitation in the DIRCM case.

1. Establishing the Normal to the Circle

To repeat the scenario, the sightline is represented by a unit vector in three-dimensional Euclidean space, and it is an assumption that successive sightlines at intervals of time trace a circle on the unit sphere. A central assertion required of the technique is that any vector that is normal to the circle and passes through its center also passes through the center of the sphere. This is easily shown by the following argument. Any point on the vector is equidistant from all points on the circle. The center of the sphere is equidistant from all points on the sphere, and so it is equidistant from any subset of points on the sphere, including the circle. Hence, a point on the vector coincides with the center of the sphere. We therefore find the set of vectors (of differing length but fixed direction) that are normal to the circle, knowing that, when projected from the origin, they pass through the center of the circle (if long enough).

The normal to a plane surface is perpendicular to all lines in the plane, and so a simple expression for the normal is

$$(\underline{r}_1 - \underline{r}_2) \times (\underline{r}_2 - \underline{r}_3) \tag{1}$$

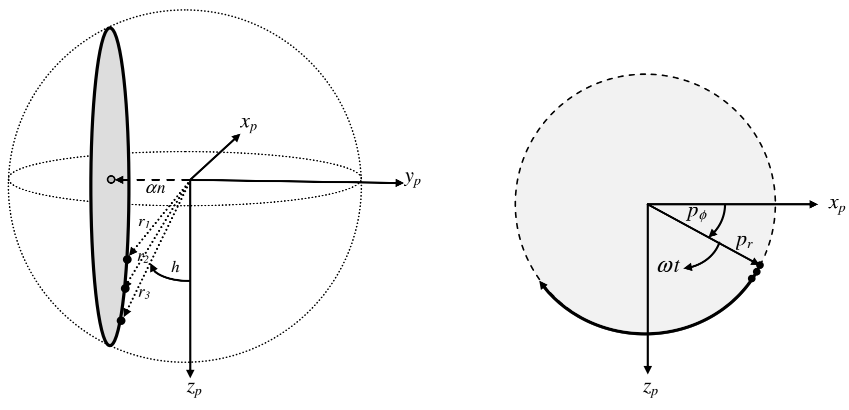

Fig. 2 Geometry for the nadir reference model: a) location of the circle plane on the unit sphere and b) expanded circle geometry.

where $\times$ denotes the vector cross product. However, this method was felt to be computationally risky, because the difference vectors are small and they are close to parallel. The approach taken was therefore to use the fact that the vector dot product of the normal and the difference vectors is zero, giving the two equations

$$\underline{n} \cdot (\underline{r}_1 - \underline{r}_2) = 0 \qquad \underline{n} \cdot (\underline{r}_2 - \underline{r}_3) = 0 \tag{2}$$

These can be solved providing the solution is nontrivial; that is,

1) The difference vectors $r_1 - r_2$ and $r_2 - r_3$ are nonzero.

2) The scalar products $n \cdot r_1$, $n \cdot r_2$, and $n \cdot r_3$ are all nonzero, noting that if one of them is zero, then they all are zero (because the origin is in the plane).

In case 1, the sightline is static and no highly dynamic approach to the nadir singularity is predicted. In case 2, the origin is in the plane and so the normal is given by the cross product of any two of the vectors (e.g., $r_1 \times r_2$). Detecting this case computationally is covered in the algorithm section presented later.

2. *Solution of the Equations*

The first point to note regarding solution of $\underline{n} \cdot (\underline{r}_1 - \underline{r}_2) = 0$ *and* $\underline{n} \cdot (\underline{r}_2 - \underline{r}_3) = 0$ is that the length of $\underline{n}$ is undefined. If $\underline{n}$ is a solution, then $\alpha\underline{n}$ (where α is any scalar) is a solution also. Therefore, if we work in Euclidean coordinates, only two of the components (n_x, n_y, n_z) are independent. An algebraic solution is obtained by dividing through by n_z (or n_y or n_z, with the divisor assumed to be nonzero) to obtain two simultaneous equations in n_x/n_z and n_y/n_z:

$$\begin{aligned} (r_{1x} - r_{2x})n_x/n_z + (r_{1y} - r_{2y})n_y/n_z &= -(r_{1z} - r_{2z}) \\ (r_{2x} - r_{3x})n_x/n_z + (r_{2y} - r_{3y})n_y/n_z &= -(r_{2z} - r_{3z}) \end{aligned} \tag{3}$$

where the measured unit length vectors are expressed in terms of their components $\underline{r}_1 = (r_{1x}, r_{1y}, r_{1z})$ and similarly for $\underline{r}_2$ and $\underline{r}_3$. These two equations are solved for the ratios n_x/n_z and n_y/n_z, and the vector direction is given by n_x/n_z, n_y/n_z, and 1. As explained later, the vector is used by scaling it so that it gives the position of the center of the circle.

This method is, however, messy to use in a computation procedure. It is not known a priori which of the three components (n_x, n_y, or n_z) is the largest (as the preferred divisor) or indeed nonzero. A convenient alternative approach is to rearrange the equations in the form $\underline{n} \cdot \underline{r}_1 = \underline{n} \cdot \underline{r}_2 = \underline{n} \cdot \underline{r}_3$ and then set each equal to an arbitrary scalar, which can be taken as unity without any loss of generality. This can be done provided that the vectors $\underline{n}$ and $\underline{r}_1$ (or $\underline{r}_2$ or $\underline{r}_3$) are not at right angles: if one is, then they all are. (If they are at right angles, then the plane includes the origin and the normal is trivially given by the cross product of any two of $\underline{r}_1$, $\underline{r}_2$, or $\underline{r}_3$.) The rearranged equations, with unity as the right-hand side, can be collected in matrix format as

$$\begin{bmatrix} r_{1x} & r_{1y} & r_{1z} \\ r_{2x} & r_{2y} & r_{2z} \\ r_{3x} & r_{3y} & r_{3z} \end{bmatrix} \begin{bmatrix} n_x \\ n_y \\ n_z \end{bmatrix} = 1 \tag{4}$$

We can now invert the matrix of the measured components of r (hereinafter called the stacked sightline matrix) to find the normal. Having defined the length of $\underline{n}$ via $\underline{n} \cdot \underline{r}_1 = \underline{n} \cdot \underline{r}_2 = \underline{n} \cdot \underline{r}_3 = 1$, it follows that there are three values to determine. The center is somewhere along the vector n, and so defining the center as at αn (where α is scalar) and using the fact that a radius of the circle is orthogonal to the normal, we have

$$(\alpha n - r_1) \cdot \alpha n = 0 \tag{5}$$

Hence, $\alpha^2 n \cdot n = \alpha n \cdot r_1$, and substituting $n \cdot r_1 = 1$ we obtain $\alpha = (n \cdot n)^{-1} = 1/\|n\|^2$. Thus, the center of the circle is located at position defined by the vector n divided by the square of its length. There are three advantages to this as a computation procedure:

1) The rank of the matrix determines whether the inverse (and hence a solution) exists and is numerically reliable.

2) The method is readily extended to the use of multiple measurements to compute a least-squares fit to the measured sightlines using the Moore–Penrose inverse and with an estimate of the reliability of the original assumption (that the sightlines lie on a circle) via the deviations of the data from the fit.

3) Using library functions, the method requires minimal coding and contains no code branches, each of which would potentially double the number of numerical test cases to be run.

3. *Numerical Considerations*

The matrix has an inverse, provided the rows (or columns) are not linearly related; if they are, the rank is less than the number of rows/columns and the inverse does not exist. Although the rank is useful in an algebraic context, exact numbers do not exist computationally, and the ability to compute an inverse depends on the determinant of the matrix being large enough for the data precision in use (e.g., 64-bit double-precision). The determinant has a simple geometric interpretation, because it is equal to $r_1 \cdot r_2 \times r_3$, which gives the volume of the parallelepiped defined by the three vectors. The value of the determinant of a matrix is unchanged by unitary transformations, which include coordinate rotations. Consequently, for the purpose of estimating the value of the determinant, points on any circular motion on the unit sphere can be reduced to the simple form given next. The plane of the circle is distance h from the origin [i.e., the nadir miss angle is $\sin(h)$]. The measurements are from successive times t_1, t_2, and t_3, and at this stage, neither the time intervals nor the rotation rate ω need be constants:

$$\begin{vmatrix} h & \sqrt{1-h^2}\cos(\omega t_1) & \sqrt{1-h^2}\sin(\omega t_1) \\ h & \sqrt{1-h^2}\cos(\omega t_2) & \sqrt{1-h^2}\sin(\omega t_2) \\ h & \sqrt{1-h^2}\cos(\omega t_3) & \sqrt{1-h^2}\sin(\omega t_3) \end{vmatrix} = h(1-h^2)[\sin(\omega t_3 - \omega t_2) + \sin(\omega t_2 - \omega t_1) - \sin(\omega t_3 - \omega t_1)] \tag{6}$$

The term in the square brackets involves the sines of the angles between radii of the circle representing each measured point, and these angles are necessarily small. For a constant rotation rate and constant time interval, we can set δ equal to the angle between successive radii, and using the power series approximation for $\sin\delta$,

$$\sin\delta = \delta - \tfrac{1}{6}\delta^3 + \tfrac{1}{120}\delta^5 + \cdots \tag{7}$$

we obtain for the determinant

$$\begin{aligned} &h(1-h^2)[2(\delta - \tfrac{1}{6}\delta^3 + \tfrac{1}{120}\delta^5) - (2\delta - \tfrac{1}{6}(2\delta)^3 + \tfrac{1}{120}(2\delta)^5)] \\ &\quad = h(1-h^2)(\delta^3 - \tfrac{1}{4}\delta^5 + \cdots) \end{aligned} \tag{8}$$

Hence, the determinant vanishes linearly as the circle approaches a great circle (i.e., the nadir pass distance approaches zero), when the circle itself collapses to a point, and as the cube of the angle between successive radii. None of these are unexpected, and in particular measurements, they have to be spaced sufficiently round the circle.

In numerical terms, for the class of system under consideration, the time interval between measurements will be typically that of a framing imager running at 50 Hz. Rotation rates below 20 deg/s are within the capability of the linear control system, and so we obtain $\delta > 7$ m $\cdot$ rad and $\delta^3 > 3.4 \times 10^{-7}$. The algorithms in use (in double-precision) operate without reporting any matrix condition issue down to a determinant of 10^{-16} and also work correctly at a smaller determinant while reporting the matrix condition number. Therefore, h must be greater than 2.9×10^{-10} rad, which is a very small angle. Conversely, smaller rotation rates are numerically acceptable.

Extending the algorithm to use more than three points improves the solution capability slightly, but then the time span (and hence span of the data round the circle) is wider. The least-squares fit allows a fit quality parameter to be computed. In practice, the finite resolution of the angle measurement and any noise corrupting the angle values is the limitation. However, if successive angles are barely distinguishable, then a nadir pass with high dynamics is not imminent. The computation compiles the stacked matrix of the sightline vectors and calculates the determinant. If it exceeds the threshold, the calculation proceeds; otherwise, the algorithm is aborted. It has been observed that only in a vanishingly small fraction of cases will the matrix inverse fail, and if required for completeness, the normal could then be calculated from the vector cross product of any two of the measured sightline vectors.

Finally, for convenient prediction of future (x, y, z) vectors and hence azimuth and elevation, the circle parameters are converted into the amplitude and phase parameters for a harmonic motion fit to the x, y, and z motions as a function of time:

$$p = p_r \sin(\omega t + p_\phi) + p_0 \tag{9}$$

where p denotes x, y, or z; p_r is the amplitude; ω is the sightline rate; p_ϕ is the initial phase; and p_0 is the offset. The azimuth and elevation angles and rates of the gimbal set are then given by

$$\begin{aligned} \eta_{\mathrm{dem}} &= \tan^{-1}(y/x) \qquad & \varepsilon_{\mathrm{dem}} &= \sin^{-1}(z) \\ \dot{\eta}_{\mathrm{dem}} &= \frac{\dot{y}x - \dot{x}y}{x^2 + y^2} \qquad & \dot{\varepsilon}_{\mathrm{dem}} &= \frac{z}{\sqrt{1 - z^2}} \end{aligned} \tag{10}$$

An example reference trajectory is shown in Fig. 3 for a 1 deg nadir miss angle h, an initial phase angle p_ϕ of 30 deg, and at an angular rate around the circular path ω of 60 deg/s from three measurements taken at 30 ms intervals approximately 1 s before the nadir pass.

The final feature of the trajectory generator is that the calculations are repeated with each new measurement, using the three most recent pairs of azimuth and elevation angles and discarding the oldest value. In this way, changes in the aircraft rotation rate are taken into account as well as the relative motion of the aircraft and target.

To illustrate the importance of the nadir geometry on the peak rate demanded from the outer gimbal, Fig. 4 shows a contour plot of the peak rate demands $\dot{\eta}_{\mathrm{dem}}$ for the OG through the nadir.

From Fig. 4 it is obvious that the OG rate demand increases dramatically the closer and faster the sightline passes the nadir: from 4 rad/s ($\dot{\eta}_{\mathrm{dem}}$) at a 5 deg miss angle (h), 20 deg/s slew rate (ω) to 615 rad/s at a 0.1 deg miss angle, and 80 deg/s slew rate and beyond. Any acceptable DIRCM nadir controller must be able to accommodate this range of motion, especially for fast-jet-mounted systems with laser defeat, which will operate in the worst case around the top left region of Fig. 4. Compare the DIRCM situation with, say, tracking of a satellite on a fixed orbit around the earth. Assuming that the orbital plane and satellite velocity remains constant, the nadir controller will operate continuously at a single point in Fig. 4, simplifying the design of an offline nadir controller. The trajectory generator presented here, however, will naturally compute the kinematic trajectory for any point in Fig. 4.

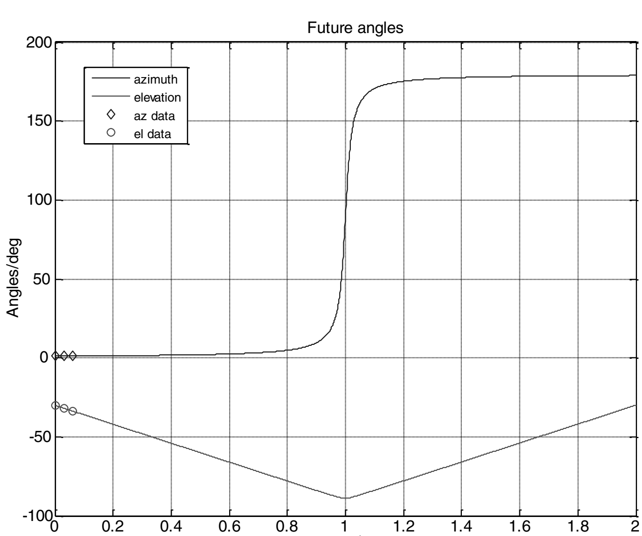

Fig. 3 Predicted nadir reference trajectory in both azimuth and elevation.

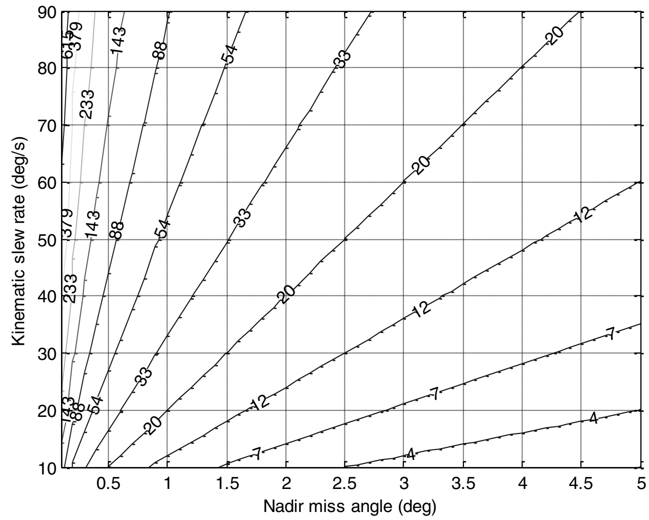

Fig. 4 Contour plot showing the peak OG rate in rad/s as a function of slew rate and nadir miss angle.

B. Individual Gimbal Axis Model

Each gimbal is actuated by a brushless dc motor driven by a pulse width modulation (Fig. 5). The integrator in the current loop proportional–integral (PI) controller provides the first fast dynamic pole in the overall model. The drive is modeled as a limited transconductance amplifier and an integrated 700 Hz current loop around the armature transfer function. Motor back-electromotive K_E and armature resistance and inductance are also modeled using simple circuit equivalence expressions for dc motors as in [12]. For the EO turret used as the baseline, a maximum rate of 33 rad/s was selected. Both rigid-body and flexible gimbal dynamics (first torsional resonance) are modeled as two rotational masses connected by a torsionally flexible shaft to give the inertial rate and position using the following equations of motion:

$$\begin{aligned} J_a \ddot{\theta}_a &= T_a - D(\dot{\theta}_a - \dot{\theta}_L) - K(\theta_a - \theta_L) \\ J_L \ddot{\theta}_L &= D(\dot{\theta}_a - \dot{\theta}_L) + K(\theta_a - \theta_L) \end{aligned} \tag{11}$$

where θ is a placeholder for either the azimuth or elevation angles and the subscripts a and L denote the motor armature and payload sides of the gimbal, respectively. The applied torque T_a is provided by the motor armature equations, and the gimbal stiffness and structural damping terms are K and D, respectively. Appropriate use of these equations yields the transfer functions between motor torque and motor rate (for the rate loop) and motor torque and payload position (for the track loop) in the form of a rigid-body term multiplied by a resonance term, as shown in Fig. 5. The gimbal inertial rate is measured by an appropriate rate gyro, the output of which provides the feedback signal for the stabilization-loop compensator, nominally designed for a 25 Hz open-loop bandwidth. The model parameters for the actual systems are obviously classified, but representative numbers are shown in Table 1.

The baseline track loop controller is a standard PI transfer function operating on the error between the desired azimuth angle η_{dem} and the measured azimuth angle, resulting in an open-loop bandwidth of 5 Hz. An additional constraint is placed on the output of the track PI limiting the rate demand to model the effects of both geared and direct-drive systems. Both track and current loop integrators have digital antiwindup around the compensator integrators.

III. MPC Guidance Controller

The purpose of the MPC guidance controller is to provide an optimal rate demand for the stabilization loop that minimizes tracking error with respect to the nadir reference. For the preceding model described with a 700 Hz current loop and less than 1 ms motor time constant, an appropriate digital controller sampling rate to capture these dynamics would exceed 3 kHz. This would require a

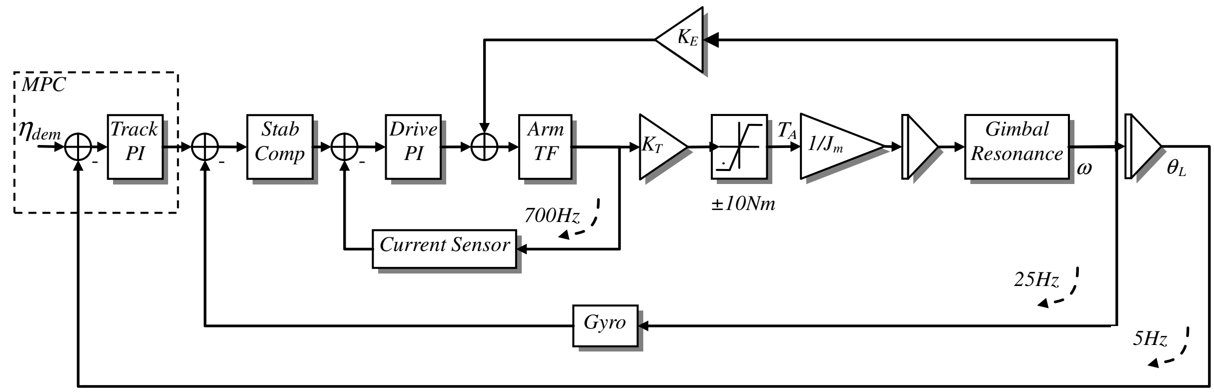

Fig. 5 Baseline azimuth axis controller block diagram; dotted box shows where the MPC controller is inserted and dashed arrows denote the bandwidths of each control loop (stab comp is the stabilization-loop compensator, drive PI is the limited transconductance amplifier, and arm TF is the armature transfer function).

prediction horizon $H_p = 300$ to cover only 0.1 s, which is a huge computational burden. Therefore, a simpler model is implemented in the MPC controller at a lower sample rate. A state-space system of the MPC model including the observer can be represented by

$$x_m(k+1) = A_m x_m(k) + B_m u_m(k) \qquad y_m(k) = C_{ym} x_m(k)$$
$$z_m(k) = C_{zm} x_m(k)$$

and

$$\begin{aligned}\hat{x}_m(k+1|k+1) &= A_m \hat{x}_m(k+1|k) + B_m u_m(k)\\ &\quad + L(y_m - C_m \hat{x}_m(k+1|k))\\ \hat{z}_m(k+1|k) &= C_{zm}\hat{x}_m(k+1|k)\end{aligned} \tag{12}$$

where $x_m(k) \in \Re^n$ is the state vector to time k, $\hat{x}_m(k+1|k) \in \Re^n$ is the state estimate at time $k+1$ using measurement information up to time k, $u_m(k) \in \Re^m$ is the input vector, $A_m \in \Re^{n\times n}$ and $B_m \in \Re^{n\times m}$ are the model state transition and control effectiveness matrices, L is the Kalman gain matrix, and (A_m, B_m) is a controllable pair (h, the subscript m denotes MPC model parameters). The main objective is to minimize the error between the controlled output $z_m(k+i|k)$ and the azimuth reference $\eta(k+i|k)$ while restricting the control input change $\Delta u_m(k+i|k)$ over a finite number of steps into the future. Here, $z_m(k+i|k)$, $\eta(k+i|k)$, and $\Delta u_m(k+i|k)$ denote the predictions made at time k of the variable z, η, and Δu at time $k+i$, based on the assumption that some sequence of inputs $u_m(k+j|k)$ $(j = 0, 1, \ldots, i\text{-}1)$ has occurred. The observer state $\hat{x}_m(k+1|k+1)$ is used as the initial condition vector for the predictor model and this action binds the prediction model with the actual plant dynamics. This is the process whereby feedback and robustness to plant/model mismatch is introduced to the controller. The cost function $V(k)$ from Maciejowski [8] is represented as

$$\begin{aligned}V(k) &= \sum_{i=H_W}^{H_p} \|\hat{z}(k+i|k) - \hat{\eta}(k+i|k)\|^2_{Q(i)}\\ &\quad + \sum_{i=0}^{H_u} \|\Delta\hat{u}(k+i|k)\|^2_{R(i)} = \|Z(k) - \boldsymbol{T}(k)\|^2_{\boldsymbol{Q}} + \|\Delta\boldsymbol{u}(k)\|^2_{\boldsymbol{R}}\end{aligned} \tag{13}$$

where H_p is the prediction horizon, H_u is the control horizon, H_w is the window parameter, and $Q(i)$ and $R(i)$ are the trajectory and control weights, respectively. Also, we define

$$\boldsymbol{Z}(k) = \begin{bmatrix}\hat{z}_m(k+H_w|k)\\ \vdots\\ \hat{z}_m(k+H_p|k)\end{bmatrix} \qquad \boldsymbol{T}(k) = \begin{bmatrix}\hat{\eta}(k+H_w|k)\\ \vdots\\ \hat{\eta}(k+H_p|k)\end{bmatrix}$$
$$\Delta\boldsymbol{u}(k) = \begin{bmatrix}\Delta\hat{u}_m(k|k)\\ \vdots\\ \Delta\hat{u}_m(k+H_u-1|k)\end{bmatrix} \tag{14}$$

To solve the problem, a prediction of the future controlled outputs $\hat{z}(k+i|k)$ is required. By defining the tracking error $E(k)$ as the difference between the reference vector and the free response of the system, the optimal set of future input now becomes [8]

$$\begin{aligned}\Delta\boldsymbol{u}_{\mathrm{opt}}(k) &= \min_{\Delta\boldsymbol{u}(k)}\left(\|\Theta\Delta\boldsymbol{u}(k) - E(k)\|^2_{\boldsymbol{Q}} + \|\Delta\boldsymbol{u}(k)\|^2_{\boldsymbol{R}}\right)\\ &\text{subject to } \Omega\Delta\boldsymbol{u}(k) \le \chi\end{aligned} \tag{15}$$

This is the standard form for a quadratic program, which is solved online. *Recall that the control signal is not used directly; rather, the computed rate signal is the desired output.*

IV. Multirate Model

Multirate controllers have been used for some time in processes in which the measurement sensor must run at a slower sample rate than the controller [13–15] (principally due to some physical limitations in the transduction process). A simple multirate scheme [14] based on successive substitution (also known as the *lifting* technique) is possible if the ratio between fast and slow rates is an integer N. This model has the same structure as that commonly used in linear model predictive control, as follows:

$$x_{\mathrm{mr}}[(k+N)T] = A^N_{\mathrm{mr}} x_{\mathrm{mr}}[kT] + B_e u_e[kT] \tag{16}$$

where $k = 0, N, 2N, \ldots$; the sample time T is the fast (gimbal model) sample rate; and the subscript mr denotes the multirate model parameters. If the control signal changes at every k, the plant model expands to

$$\begin{bmatrix}x_{\mathrm{mr}}[(k+1)T]\\ x_{\mathrm{mr}}[(k+2)T]\\ \vdots\\ x_{\mathrm{mr}}[(k+N)T]\end{bmatrix} = \begin{bmatrix}A_{\mathrm{mr}}\\ A^2_{\mathrm{mr}}\\ \vdots\\ A^N_{\mathrm{mr}}\end{bmatrix} x_{\mathrm{mr}}[(k)T] + \begin{bmatrix}B_{\mathrm{mr}} & 0 & 0 & 0\\ A_{\mathrm{mr}}B_{\mathrm{mr}} & B_{\mathrm{mr}} & 0 & 0\\ \vdots & \vdots & \ddots & 0\\ A^{N-1}_{\mathrm{mr}}B_{\mathrm{mr}} & A^{N-2}_{\mathrm{mr}}B_{\mathrm{mr}} & \cdots & B_{\mathrm{mr}}\end{bmatrix}\begin{bmatrix}u[(kT)]\\ u[(k+1)T]\\ \vdots\\ u[(k+N)T]\end{bmatrix} \tag{17}$$

Table 1 Simulation parameters

Model parameters	Numerical values
(J_a, J_L)	$(1e-4, 0.7)$ kg · m^2
(K, D)	(1.5e3 Nm/rad, 30 Nms/rad)
(K_T, K_E)	(0.56, 0.56)
$(K_p, K_i)_{\mathrm{track}}$	(15, 200)
$(K_p, K_i)_{\mathrm{rate}}$	(60, 400)
$(K_p, K_i)_{\mathrm{current}}$	(20, 15,000)

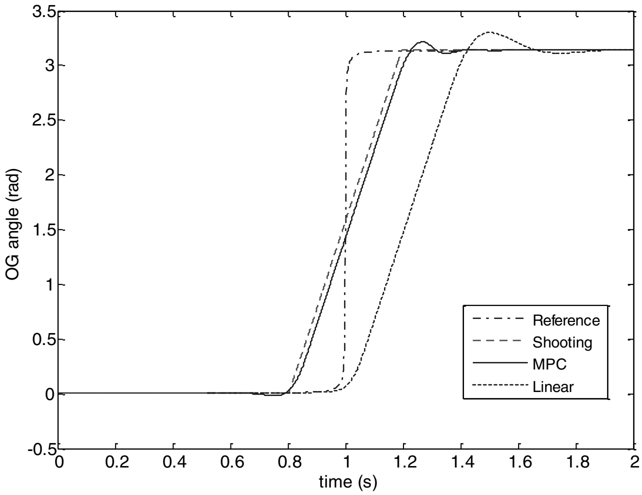

Fig. 6 Comparison of MPC, shooting, and baseline linear controllers for 0.1 deg nadir pass.

It is a simple exercise to show that the generic multirate sample model reduces to this form.

V. Results and Analysis

To test both the performance and robustness of the guidance MPC approach to plant/model mismatch, the simplest possible MPC model (the double integrator) was chosen:

$$\dot{x}_m = \begin{bmatrix} \dot{\eta}_m \\ \dot{\omega}_m \end{bmatrix} = \begin{bmatrix} 0 & 1 \\ 0 & 0 \end{bmatrix} \begin{bmatrix} \eta_m \\ \omega_m \end{bmatrix} + \begin{bmatrix} 0 \\ 10 \end{bmatrix} u_m \qquad y_m = [1 \quad 0] x_m \tag{18}$$

The input and rate signals were constrained to $-10 \leq u_m \leq 10\ \mathrm{N \cdot m}$ and $-10 \leq \omega_m \leq 10\ \mathrm{rad/s}$, respectively. The MPC prediction and control horizons were $H_p = 100$ and $H_u = 10$, respectively, and the slow sample rate was 100 Hz. With the gimbal model running at 3 kHz, this gives an N of 100 and a prediction horizon of 1 s. Recall that the full simulation also includes gimbal resonance, dc motor armature current dynamics, and current loop dynamics, which is significantly different from the simple MPC model. A comparison of this controller with the standard linear PI for an 0.1 deg nadir pass at 60 deg/s is shown in Fig. 6.

From Fig. 6, the effect of preview by the MPC controller is evident, as is the upper rate limit on the gimbal response. It is clear that the MPC controller settles back into the accurate track sooner than the baseline. Also evident is that there appears to be no tangible loss of performance due to the use of a simplified plant model in the MPC design. There is a slight ripple as the controller recaptures the kinematic trajectory after the nadir, but this is due solely to the difference between the internal plant model and the system model (if the MPC controller in the multirate configuration is used to control a plant with the same dynamics as the internal plant model, this effect is not present). Figure 6 also contains an optimal shooting trajectory designed to minimize the integral-squared tracking error for a rate-limited system and calculated offline for the specific nadir geometry of Fig. 6. It can be easily seen that the MPC controller has attained very near-optimal nadir tracking with all of the optimization performed online.

However, this response does not demonstrate whether receding-horizon control would provide tangible operational improvements; to be certain, one must examine the error profiles for a range of nadir pass angles. This is shown in Fig. 7 for pass angles of 0.1, 1, 5, and 10 deg. Also shown is the field of view of the sensor to illustrate when image tracking is impossible.

MPC successfully reduces the overall tracking error for all cases. This is most evident from Fig. 7c, in which the MPC controller keeps the missile within the sensor field of view and the baseline controller loses track for 0.3 s. There is, however, an issue regarding the operational impact of the MPC-induced loss of track *before* the nadir, as seen in Figs. 7a and 7b.

To quantify the overall operational performance improvement, the tests were rerun with a lower beam divergence to represent the jammer signal. The system may then be defined as operational (i.e.,

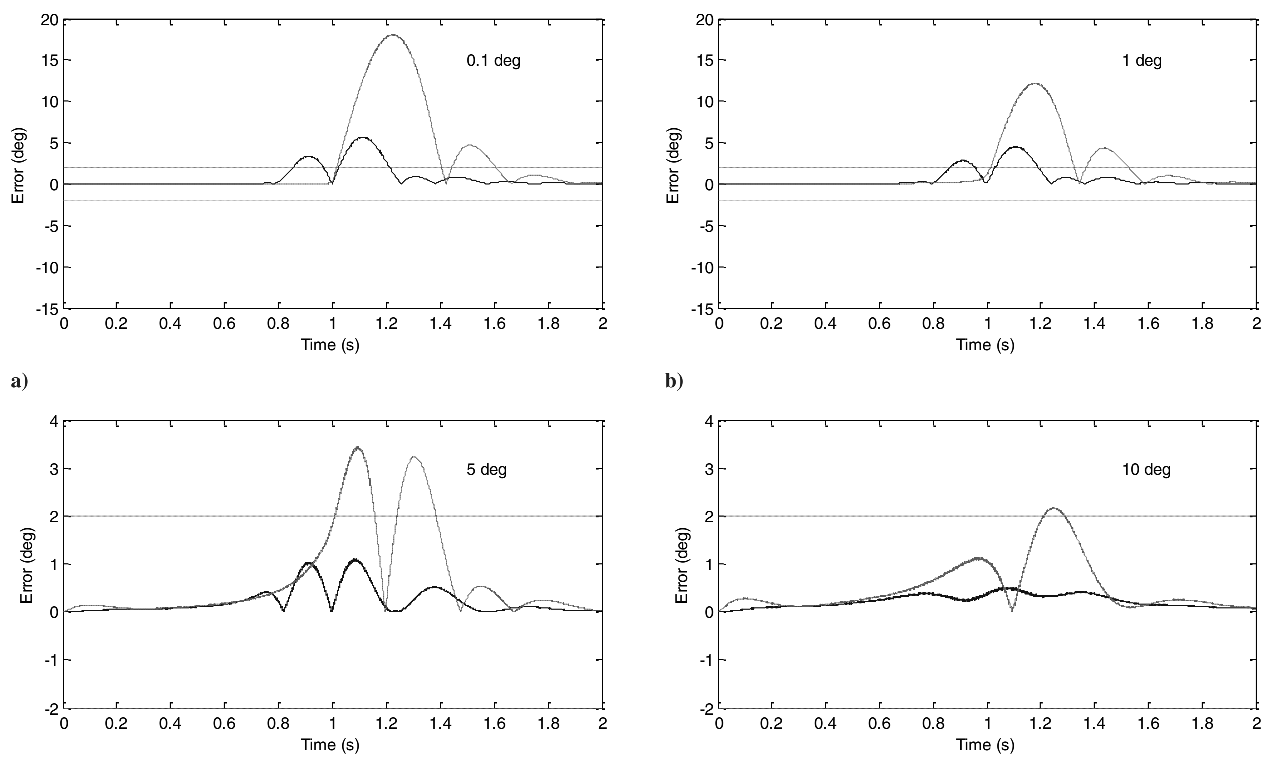

Fig. 7 Tracking errors for MPC and baseline controllers for nadir passes of a) 0.1 deg, b) 1 deg, c) 5 deg, and d) 10 deg; camera instantaneous field of view (dashed) is also shown.

Table 2 Total time for which system is operationally inactive for nadir miss angles

	0.1 deg	1 deg	5 deg	10 deg
MPC	0.3 s	0.25 s	0 s	0 s
Linear	0.55 s	0.47 s	0.29 s	0.08 s

capable of delivering a defeat signal) when the tracking error is less than this bound. Table 2 shows the total time that the sightline exceeds the operational limits over a set of nadir passes with a 60 deg slew rate for both MPC and linear controllers.

It is obvious from Table 2 that the MPC controller provides an (almost) constant 0.25 s additional time on target, which represents a significant proportion of the effective jamming time for a typical DIRCM engagement. There are therefore real operational benefits to employing an MPC controller around the nadir.

VI. Conclusions

A new method for implementing the benefits of model predictive control within an electro-optic system track loop is presented. By using the new guidance MPC formulation, optimal trajectory generation is achievable with a simple model, giving a new method for implementing fast model predictive control. Simulation tests of the model predictive controller around the nadir show that the new controller outperforms the baseline linear controller on all performance metrics and that the new controller will also yield a near-optimal solution to the nadir control problem. Significant potential operational benefits are demonstrated. This result justifies the pursuit of more complex nonlinear predictive algorithms for the directed infrared countermeasures application.

References

[1] Thomson, G., "Advances in Electro-Optic Systems for Targeting," *Proceedings of the Institution of Mechanical Engineers, Part G (Journal of Aerospace Engineering)*, Vol. 212, No. 1, 1998, pp. 1–19. doi:10.1243/0954410981532090

[2] Rue, A. K., "Stabilisation of Precision Electro-Optical Pointing and Tracking Systems," IEEE Transactions of Aerospace Electronic Systems, Vol. 5, No. 5, 1969, pp. 805–819.

[3] Borkowski, K. M., "Analytic Derivation of Various Properties of the Zenith Keyhole," *Acta Astronomica*, Vol. 37, June 1987, pp. 79–88.

[4] Crawford, P. S., and Brush, R. J. H., "Trajectory Optimisation to Minimise Antenna Pointing Error," *Computing and Control Engineering Journal*, Vol. 6, No. 2, 1995, pp. 61–67. doi:10.1049/cce:19950201

[5] Bai, M. W., Kingston, K. A., Malone, H. R., Dogget, J. G., Vidano, R. P., and Yingling, E. R., "Method and Apparatus for Eliminating Keyhole Problem of an Azimuth-Elevation Gimbal Antenna," U.S. Patent 6,285,338 B1, 4 Sept. 2001.

[6] Skoglar, P., "Modelling and Control of IR/EO-Gimbal for UAV Surveillance Applications," M.Sc. Thesis, Department of Electrical Engineering, Linköping Univ., Linköping, Sweden, 2002.

[7] Kim, J., Marani, G., Chung, W. K., and Yuh, J., "Task Reconstruction Method for Real-Time Singularity Avoidance for Robotic Manipulators," *Advanced Robotics*, Vol. 20, No. 4, Apr. 2006, pp. 453–481.

[8] Maciejowski, J. M., *Predictive Control with Constraints*, Prentice–Hall, Upper Saddle River, NJ, 2002.

[9] Kouvaritakis, B., Cannon, M., Rossiter, J. A., "Nonlinear Model Based Predictive Control," *International Journal of Control*, Vol. 72, No. 10, 1999, pp. 919–928. doi:10.1080/002071799220650

[10] Bemporad, A., Morari, M., Dua, V., Pistikopoulos, E. N., "The Explicit Linear Quadratic Regulator for Constrained Systems," *Automatica*, Vol. 38, No. 1, 2002, pp. 3–20. doi:10.1016/S0005-1098(01)00174-1

[11] Kouvaritakis, B., Cannon, M., Rossiter, J. A., "Who Needs QP for Linear MPC Anyway?," *Automatica*, Vol. 38, No. 5, 2002, pp. 879–884. doi:10.1016/S0005-1098(01)00263-1

[12] Hughes, A., *Electric Motors and Drives: Fundamentals, Types and Applications*, 2nd ed., Newnes, , Oxford, 1998.

[13] Halldorsson, U., Fikar, M., and Unbehauen, H., "Multirate Nonlinear Predictive Control," *American Control Conference*, Inst. of Electrical and Electronics Engineers, Piscataway, NJ, May 2002, pp. 4191–4196.

[14] Fujimoto, H., and Hori, Y., "High-Performance Servo Systems Based on Multirate Sampling Control," *Control Engineering Practice*, Vol. 10, No. 7, 2002, pp. 773–781. doi:10.1016/S0967-0661(02)00010-2

[15] Armesto, L., Tornero, J., and Tomizuka, M., "Multi-Rate Control Systems with Multirate Model-Based Holds and Observers," *IEEE Conference on Control Applications*, Inst. of Electrical and Electronics Engineers, Piscataway, NJ, Sept. 2004.